Preconditioned GIFFT: A Fast MoM Solver for Large Arrays of Printed Antennas

(*Invited Paper*)

[1,2] B. J. Fasenfest, [1,3] F. Capolino, and [1] D. R. Wilton
[1] Department of Electrical and Computer Engineering, University of Houston, Houston TX, USA
(e-mail: capolino@dii.unisi.it, wilton@uh.edu)
[2] Lawrence Livermore National Laboratory, Livermore, CA, USA
[3] Department of Information Engineering, University of Siena, 53100 Siena, Italy

***Abstract*—** A new type of fast method of moments (MoM) solution scheme using standard basis functions for large arrays with arbitrary contours and/or missing elements is applied to array antennas in a layered configuration. The efficiency of the method relies on use of the FFT along with approximating the Green's function as a separable sum of interpolation functions defined on a relatively sparse, uniform grid. The method is ideally suited for solving array problems, and its effectiveness is demonstrated here for planar arrays of printed antennas. Both fill and solve times, as well as memory requirements, are dramatically improved with respect to standard MoM solvers.

***Index Terms*—**Array antennas, fast solvers, method of moments, periodic structures.

I. INTRODUCTION

A straightforward numerical analysis of large arrays requires significant memory storage and long computation times. Several techniques are currently under development to reduce this cost. One such technique is the GIFFT (Green's function interpolation and FFT) method [1] that belongs to the class of fast solvers for large structures. This method uses a modification of the standard AIM approach [2] that takes into account the reusability properties of matrices that arise from identical array elements. Like the methods presented in [3]-[6], the GIFFT algorithm is an extension of the AIM method in that it uses basis-function projections onto a rectangular grid of Green's function samples that are interpolated with Lagrange interpolating polynomials. The use of a rectangular grid results in a matrix-vector product involving the Green's function samples that is convolutional in form and can thus be evaluated using FFTs. Although our method differs from [3]-[6] in various respects, the primary differences between the AIM approach [2] and the GIFFT method [1] is the latter's use of interpolation to represent the Green's function (GF) and its specialization to periodic structures by taking into account the reusability properties of matrices that arise from interactions between identical cell elements.

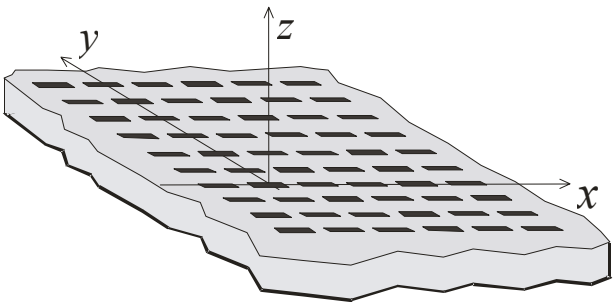

Fig. 1. Array of dipoles excited by delta gap voltage generators on an infinite grounded dielectric slab.

It should be mentioned that fast multipole methods (FMM) [7]-[9] have also been effectively applied to model large structures. In addition, a general numerical scheme has been introduced in [10] that use FMM to determine the coupling between periodic cells, with the interior of each cell being analyzed by the finite element method. To reduce the fill and solve time, other algorithms have been developed that use periodicity-induced physical properties. For example, the methods in [11], [12] use an a priori estimate of the fields scattered by truncated arrays, which behave as Floquet-modulated-diffracted fields [13], to construct global basis functions.

The present work reports performances of the GIFFT method for the cases of conducting dipole antennas in free space and printed on a dielectric grounded slab (Fig. 1), and for patch antennas fed by aperture slots excited by microstrip lines (Fig. 2). For these cases, the Lagrange interpolation scheme is applied to the layered material dyadic Green's function for the mixed potential integral equation [14]. Furthermore, a multi-region interaction is considered since magnetic current unknowns are located on both sides of a shorted screen separating the two regions on either side of the slot (Fig. 2). A block

preconditioning scheme is implemented to greatly reduce the number of iterations required for a solution. If the array consists of planar conducting bodies, the array elements are meshed using standard subdomain basis functions for triangles [15]; the same bases may be used in the apertures where magnetic unknowns are defined. The GIFFT algorithm has been implemented in the standard method of moments (MoM) code EIGER$_{TM}$ [16]. In our implementation, the array boundaries are not restricted to be rectangular, and the array excitation can be arbitrary.

The method greatly reduces solution time by speeding up the computation of matrix-vector products needed in iterative solutions. The GIFFT approach also reduces fill time and memory requirements since the sparse interpolation can be used for all but near element interactions.

II. FEED REGION AND RADIATION REGION: DEFINITION OF INTERPOLATION DOMAIN

The antenna structures analyzed in this paper are shown in Figs. 1 and 2. In Fig. 1 an array antenna of M conducting dipoles is printed on a grounded dielectric substrate. The dipoles are fed by delta gap generators and meshed with triangles that form the sub-domains of triangle surface patch basis functions. Voltage generators $V_g^{\mathbf{p}}$, with $\mathbf{p}=(p_1,p_2)$ a generic double index, are defined for all the dipoles.

In the second example, illustrated in Fig. 2, the region above the ground plane may include a multilayered substrate with M conducting patches fed by slots. Below each slot the microstrip line feeding each antenna is assumed not to interfere with the feed networks of other patches. Mutual coupling between the patches and the slots is considered in the region above the ground plane. Hence, the only model approximation is to neglect coupling between the microstrip lines and slots in the region below the ground plane.

The multiport analysis that one may obtain from this approach may subsequently be used as a multiport equivalent network for designing (or refining) the actual feed network. Array scan blindness, grating lobes and array edge effects are correctly taken into account since they are produced by the mutual coupling above the ground plane. In Fig. 2, voltage generators $V_g^{\mathbf{p}}$ are defined on the microstrip lines below every slot. Concerning notation, as shown in Figs. 1 and 2, the array is decomposed into blocks of elements with each element denoted by the two-component multi-index $\mathbf{p}$; a prime is added to distinguish source from observation element locations ($\mathbf{p}'=(p_1',p_2')$). Within each block representing an element, the electric and magnetic currents are expressed in terms of the usual divergence-conforming basis functions $\Lambda_n^{\mathbf{p}'}$. The m-indexed test functions are denoted by $\Lambda_m^{\mathbf{p}}$ (see [1] for more details).

In solving the system, the vanishing of the tangential electric field is imposed on every conducting patch in Fig. 1, leading to the discretized electric field integral equation (EFIE) defined in the standard way (see also [1])

$$\left[Z_{mn}^{\mathbf{p}\mathbf{p}'+} \right]\left[\mathrm{I}_n^{\mathbf{p}'} \right] = \left[V_{\mathrm{g},m}^{\mathbf{p}} \right] \tag{1}$$

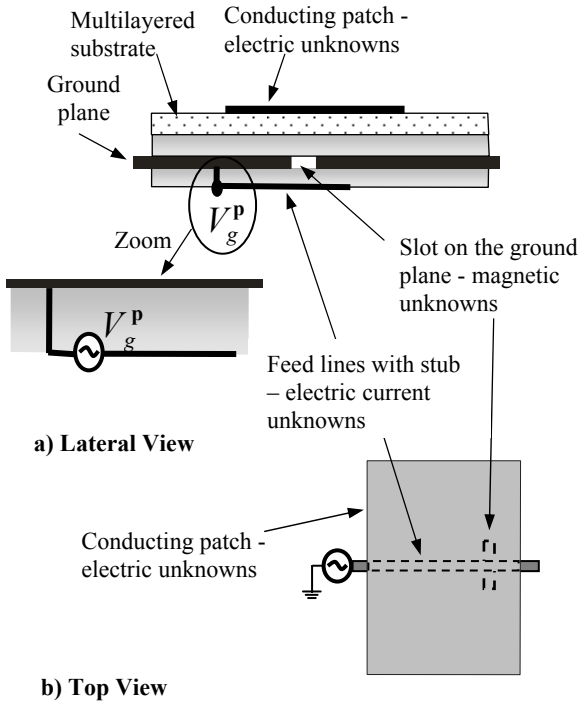

Fig. 2. Single array element of an array of printed antennas in a multilayered environment. (a) Lateral view; (b) Top view. The ***p***th element is fed by an independent microstrip line excited by a voltage $V_g^{\mathbf{p}}$ ($\mathbf{p}$=(p_1,p_2) is a double index). The array elements are coupled via the region above the ground plane. Identical feed lines for each array antenna are assumed uncoupled; hence the Green's function is interpolated only in the region above the ground plane.

where $\left[\mathrm{I}_n^{\mathbf{p}'} \right]$ are the weights of the electric unknowns defined on each $\mathbf{p}$ th dipole and $V_{g,m}^{\mathbf{p}}$ are the voltage generators. For the geometry in Fig. 2 the magnetic currents provide continuity of the electric field, and we impose continuity of the magnetic field (MFIE) on each of the M slots. Therefore, electric unknowns are defined on the patch ($\left[\mathrm{I}_n^{\mathbf{p}'} \right]$) and microstrip ($\left[\bar{\mathrm{I}}_n^{\mathbf{p}'} \right]$) while

magnetic unknowns $\left[V_n^{\mathbf{p}'}\right]$ are placed on the slots, resulting in the system equation

$$\begin{pmatrix} \left[Z_{mn}^{\mathbf{pp}'+}\right] & 0 & \left[-\beta_{mn}^{\mathbf{pp}'+}\right] \\ 0 & 0 & 0 \\ \left[\beta_{mn}^{\mathbf{pp}'+}\right] & 0 & \left[Y_{mn}^{\mathbf{pp}'+}\right] \end{pmatrix} \begin{pmatrix} \left[\mathrm{I}_n^{\mathbf{p}'}\right] \\ \left[\overline{\mathrm{I}}_n^{\mathbf{p}'}\right] \\ \left[V_n^{\mathbf{p}'}\right] \end{pmatrix} + \delta_{\mathbf{p},\mathbf{p}'} \begin{pmatrix} 0 & 0 & 0 \\ 0 & \left[Z_{mn}^{-}\right] & \left[-\beta_{mn}^{-}\right] \\ 0 & \left[\beta_{mn}^{-}\right] & \left[Y_{mn}^{-}\right] \end{pmatrix} \begin{pmatrix} \left[\mathrm{I}_n^{\mathbf{p}'}\right] \\ \left[\overline{\mathrm{I}}_n^{\mathbf{p}'}\right] \\ \left[V_n^{\mathbf{p}'}\right] \end{pmatrix} = \begin{pmatrix} 0 \\ \left[V_{\mathrm{g},m}^{\mathbf{p}}\right] \\ 0 \end{pmatrix}. \tag{2}$$

The + or – superscripts denote operators for regions above or below the ground plane. The matrix $Z_{mn}^{\mathbf{pp}'}$ is the EFIE operator connecting blocks $\mathbf{p}$ and $\mathbf{p}'$, and $Y_{mn}^{\mathbf{pp}'}$ is its dual, representing the magnetic field due to magnetic current sources; $\beta_{mn}^{\mathbf{pp}'}$ is the corresponding magnetic field integral equation (MFIE) operator. Subscripts m and n index testing and basis functions within cells $\mathbf{p}$ and $\mathbf{p}'$, respectively, and the matrix vector products in (1), (2) sum over the indices m

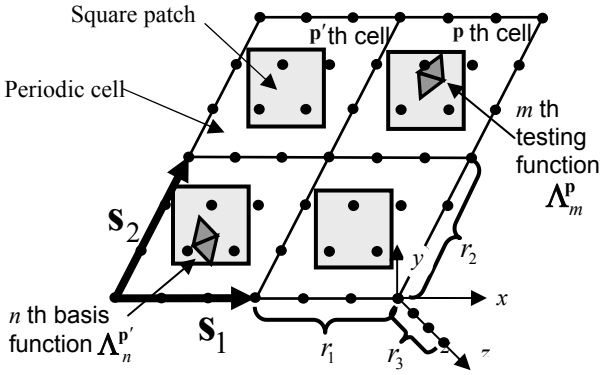

Fig. 3. Array cell index definitions and arbitrary skew lattice vectors $\mathbf{s}_1, \mathbf{s}_2$. The periodic grid on which the Green's function is evaluated and sampled is shown superimposed on the array cells. Within an array cell, the Green's function is evaluated at $r_1 \times r_2 \times r_3$ points. The square-shape darker regions represent conductors within the array cells.

and $\mathbf{p}' = (p_1', p_2')$. The corresponding matrices Z_{mn}^{-}, Y_{mn}^{-}, and β_{mn}^{-} that appear only on diagonal blocks represent the coupling to the structures below the ground plane for each array element; they affect only the $\mathbf{p} = \mathbf{p}'$ self blocks because the Kronecker delta $\delta_{\mathbf{p},\mathbf{p}'} = 1$ for $\mathbf{p} = \mathbf{p}'$, and $\delta_{\mathbf{p},\mathbf{p}'} = 0$ for $\mathbf{p} \neq \mathbf{p}'$. Note that the number of blocks in the first matrix in (2) grows as the square of the number of array elements while the size of the second matrix remains the same for any number of array elements.

Using standard MoM, the matrix in (1) or the first matrix in (2) has huge memory, fill, and solve time requirements for large arrays. This computational difficulty arises from the top region because of the coupling between even widely separated array elements that in most situations cannot be neglected. The numerical burden is reduced by applying GIFFT to this region. That is, the Green's function terms in this region are sampled and interpolated as shown below, and the matrix vector product for the majority of the system is accelerated by using the FFT.

III. THE GIFFT METHOD

For simplicity we show the basic idea of the GIFFT method only for the EFIE, i.e., the moment matrix-vector for the original discretized EFIE in (1). Analogous concepts apply to the other operators $\beta_{mn}^{\mathbf{pp}'+}$ and $Y_{mn}^{\mathbf{pp}'+}$ involved in (2). Thus, (1) or the first block product from the left matrix of (2), is written as [1]

$$\left[Z_{mn}^{\mathbf{pp}'}\right]\left[\mathrm{I}_n^{\mathbf{p}'}\right] = \left[\Delta Z_{mn}^{\mathbf{pp}'}\right]\left[\mathrm{I}_n^{\mathbf{p}'}\right] + \left[\tilde{Z}_{mn}^{\mathbf{pp}'}\right]\left[\mathrm{I}_n^{\mathbf{p}'}\right] \tag{3}$$

where $\tilde{Z}_{mn}^{\mathbf{pp}'}$ denotes matrix elements approximated via the interpolation scheme. The interpolation, however, is inaccurate for nearby cells, which require the correction matrix $\Delta Z_{mn}^{\mathbf{pp}'} = Z_{mn}^{\mathbf{pp}'} - \tilde{Z}_{mn}^{\mathbf{pp}'}$. The correction matrix is a block Toeplitz difference matrix that may be taken as zero for elements whose indices satisfy $|p_1 - p_1'| \geq c_1$ and $|p_2 - p_2'| \geq c_2$ for some constants (c_1, c_2); hence it is sparse. Furthermore, it is constructed from a single computation on a stencil of cells consisting of an observation cell and adjacent cells. The m-indexed test functions are denoted by $\Lambda_m^{\mathbf{p}}$ (see [1] for more details.) To evaluate the matrix/vector product, we note that $\left[\Delta Z_{mn}^{\mathbf{pp}'}\right]\left[\mathrm{I}_n^{\mathbf{p}'}\right]$ is quickly computed since $\Delta Z_{mn}^{\mathbf{pp}'}$ is sparse, whereas $\left[\tilde{Z}_{mn}^{\mathbf{pp}'}\right]\left[\mathrm{I}_n^{\mathbf{p}'}\right]$ is of convolutional form and can be evaluated using a 2D FFT as follows [1]:

$$\left[\tilde{Z}_{mn}^{\mathbf{pp}'}\right]\left[\mathrm{I}_n^{\mathbf{p}'}\right] = \sum_{\mathbf{i},j,j'} < \Lambda_m^{\mathbf{p}}, L_{\mathbf{i}} L_j > \cdot \mathsf{MASK}_{\mathbf{i}}\, \mathsf{FFT}_{\mathbf{i}}^{-1} \cdot \left[\left(\mathsf{FFT}_{\mathbf{i}}\, \overline{\overline{\mathcal{G}_{\mathbf{i},j,j'}^{\mathrm{E}}}} \right) \cdot \mathsf{FFT}_{\mathbf{i}} \left(\overline{\overline{\sum_{\mathbf{p}'} \sum_{n=1}^{N} < L_{\mathbf{i}} L_{j'}, \Lambda_n^{\mathbf{p}'} > \mathrm{I}_n^{\mathbf{p}'}}} \right) \right] \tag{4}$$

where $\mathbf{i}, j$ and $\mathbf{i}', j'$ denote periodic grid points for the Green's function evaluations (Fig. 3), and the double bars

over a quantity indicate that its length is extended so as to obtain a circular convolutional form and then zero-padded to obtain vectors of length 2^k for efficient application of the fast Fourier transform (FFT); FFT^{-1} denotes the inverse fast Fourier transform, and $\mathsf{MASK}_{\mathbf{i}}$ is the array mask restricting the result to array elements within the array boundary. $<\mathbf{\Lambda}^{\mathbf{p}}_m, L_{\mathbf{i}}L_j>$ is the projection of the mth basis function in the $\mathbf{p}$th array cell onto the Lagrange polynomial $L_{\mathbf{i}}L_j$ interpolating the $\mathbf{i}, j$ th point. $\mathcal{G}^{\mathrm{E}}_{\mathbf{i},j,j'}$ represents the sampled Green's electric field dyad (though in reality the field is calculated in mixed-potential form). Since vector basis functions are used, $<\mathbf{\Lambda}^{\mathbf{p}}_m, L_{\mathbf{i}}L_j>$ is a vector. For arrays made of nonplanar scatterers in free space the FFT algorithm is applied to the interpolation points along *z*, while for layered media the FFT is only applied along the two transverse directions $\mathbf{S}_1$ and $\mathbf{S}_2$ along the planar array.

In homogeneous media, the dyad can be expressed in terms of a single scalar potential. For layered material, however, the far interactions require the computation and storage of the five non-zero components of the magnetic vector potential Green's dyad and two scalar potentials for all possible interactions between interpolating points in at most two planes separated in the *z* dimension, and for all unique discrete separations in the transverse dimension. There is a very high cost of computing these seven Green's potentials compared to the homogeneous medium case, but this cost is dramatically reduced by first generating the potentials at a suitable set of sample points along radial lines in each source plane representing possible source/observation point separations in the transverse dimension. Potential values between sample points along the sampling line are accurately generated via a non-rational interpolation scheme. Along any other radial line, potentials having the same separation can be constructed from those along the sampling line simply by multiplying by factors involving at most cosines or sines of the angle from the sampling line. The Green's function values along the sampling line are thus used to generate values on the regular grid by interpolation; in turn, a second level of interpolation on the grid is employed in the GIFFT algorithm. The increased number of potential components increases memory requirements when layered media are present, but does not increase the number of FFT's that must be performed per iteration. Furthermore, the Green's potential samples themselves are transformed only once, before any iterations are performed. During each iteration, the updated current coefficients are projected onto the interpolating grid as usual. Once the projections are transformed into the spectral domain, then a single matrix vector multiplication for each dyadic component of the Green's function must be performed. The inverse transform is then computed to complete the iteration step. Assuming *N* interpolation points, the number of multiplications in the spectral domain is O(*N*) while the FFT operation is O($N \log N$). Hence, the presence of the extra Green's function terms does not greatly slow the iteration.

IV. BLOCK DIAGONAL PRECONDITIONER

When using an iterative solver such as BiCGStab on a very large matrix system, the solution may converge very slowly if conditioning is poor. For this reason, a preconditioner is needed to improve the solution time. Since many arrays are designed to minimize mutual coupling between array elements, a block diagonal preconditioner for an array seems a logical and simple choice. This preconditioner consists of the self-cell interaction terms of the impedance matrix only. The inverse of this matrix is also a block-diagonal matrix and contains the inverse of the self-array cell blocks $\left[Z^{\mathbf{pp}'}_{mn}\right]$, with $\mathbf{p}=\mathbf{p}'$. Physically, this preconditioner solves the original problem as if there were no interaction between array cells. For array designs with little mutual coupling this is a very good assumption and often only a handful of iterations are required. For arrays with strong coupling some deterioration in performance is to be expected. Because an accurate computation of the self block is needed for the near interaction corrections, this preconditioner does not require additional setup time. The cost of inverting a self block is also negligible since the number of unknowns involved is small compared to the overall array size. Thus after each matrix-vector product is computed during an iteration, the resulting vector is multiplied by the preconditioner, adding an O(MN^2) computation to the total time for the matrix vector product (*M* is the number of array elements and *N* is the number of degrees of freedom in each array cell.)

V. RESULTS

Four different test arrays geometries were simulated and the results of the GIFFT method, both with and without preconditioning, were compared to an "exact" MoM solution of these arrays. The "exact" solution does not use interpolation or fast multiplication, but does utilize the Toeplitz nature of the matrices to speed fill time and reduce storage.

A. Array of Dipoles

The first two arrays consist of 20×20 elements with a lattice spacing $S_1 = S_2 = 0.5\lambda_0$, where λ_0 is the free space wavelength, in both *x* and *y* directions. Each dipole is fed by a delta gap source at its center. Each dipole

contains 23 unknowns and is $0.39\lambda_0$ long and $0.01\lambda_0$ wide. In the first test case the dipoles are in free space, while in the second one the same dipoles are printed on a grounded dielectric slab as in Fig. 1. The height of the dielectric slab is $d = 0.19\lambda_0$ and its relative permittivity is $\varepsilon_r = 2.55$, as for the case treated in [17]. Both these cases used fourth order interpolation of the Green's Function in both transverse directions. The GF is thus sampled at five points in each direction, resulting in $r_1 \times r_2 = 5 \times 5 = 25$ points for each array cell. Interpolation points are also distributed along the border of an array cell and are thus shared by contiguous cells, so the computational burden is determined by the evaluation and storage of the various GF components for only 16 distinct points per array cell.

The third case analyzed consists of an array of 25×25 square conducting patches in free space illuminated by a plane wave at 6 GHz incident from a direction perpendicular to the array plane. The patches are 11.4 [mm] on a side with a separation of 3.8 [mm] between patches, and thus the lattice spacings are $S_1 = S_2$ =15.2 [mm]. Each patch was meshed using triangles, creating 65 unknowns per patch. This GIFFT method used fifth order (25 distinct points per cell) interpolating polynomials in both planar directions.

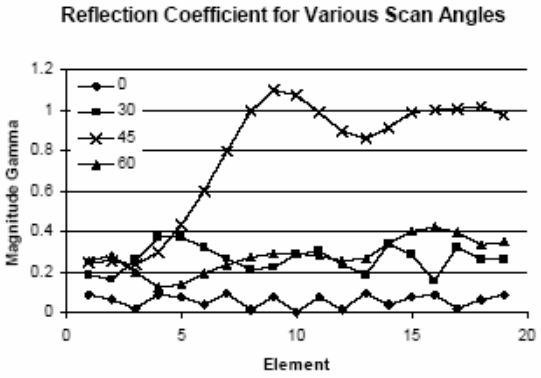

Fig. 4. Active reflection coefficients for various scan angles on the E-plane for an array of 19 x 19 dipoles on a grounded dielectric slab. Scan blindness occurs for $\theta = 45.8°$.

Table 1 shows the run times for the standard MoM and GIFFT solutions of the three arrays, as well as the error in the GIFFT solution compared to that of the standard MoM, which takes advantage of the Toeplitz storage that also reduces the fill time. It can be clearly seen that the GIFFT method offers a dramatic savings in both fill and solve times while maintaining a high level of accuracy that is evaluated as the average of the relative errors over all the unknowns. It can also be seen that use of the preconditioner dramatically reduces the number of BiCGstab iterations needed for a solution, further reducing solution time. The BiCGstab iterations are stopped when the solution error determined by the algorithm is lower than 10^{-4}. The GIFFT method also dramatically reduces the memory storage requirements. For example, for the 25×25 square patch array (M = 625 array cells), each patch was discretized using N=65 basis functions, requiring storage of $N \times N$ =4225 complex numbers for *each* $\mathbf{p}, \mathbf{p}'$ block $\left[Z_{mn}^{\mathbf{pp}'} \right]$ of the full impedance matrix. Instead, using GIFFT with a fifth order interpolation scheme, we need to store only 36 Green's function samples per array cell. Interpolation points are also distributed along the border of an array cell and are thus shared by contiguous cells resulting in 25 *distinct* sampling points per array cell. GIFFT's storage advantage is further amplified by the fact that if there are M = 625 array cells in a square array, there are M^2 matrix blocks in the complete matrix, while there are only about $4M$ blocks of sampled Green's function points. The factor four arises from extending the evaluation domain of the Green's function to consider all possible interactions on the actual array as shown in [1, Fig. 3]. For the 25×25 array, this means that the system matrix for a standard solution must contain about $N^2 \times M^2 = 1.65 \times 10^9$ complex entries (that reduce to $N^2 \times (2M - 1) = 5.28 \times 10^6$ when stored in the Toeplitz format), while there are only $25 \times 4 \times M = 62.5 \times 10^3$ entries in the sampled Green's function array in free space. As explained in Sec. III, for layered media, the number of the GIFFT complex samples must be multiplied by seven, the number of unique dyadic and scalar potential terms used in the mixed potential formulation.

The results in Fig. 4 are related to an array of 19×19 (to match the results in [17]) dipole elements on the same grounded dielectric slab considered before ($d = 0.19\lambda_0$, $\varepsilon_r = 2.55$) that exhibits scan blindness in the E-plane at $\theta = 45.8°$ [17], [18]. Therefore the dipoles are fed with a linear progressive phase along x so as to scan the array beam along the θ direction in the E-plane (the x-z plane in Fig. 1). The active reflection coefficients for the center row of array elements are shown for various scan angles. As pointed out in [17], the results show that for a broadside scan angle $\theta = 0°$ the reflection coefficients are symmetric with respect to the center element (the 10 th) that is well matched, i.e., the magnitude of the reflection coefficient is much less than unity. This verifies that the antenna elements have been matched to the input impedance of the center element at broadside. When the array is scanned to $\theta = 45°$, the reflection coefficient varies considerably across the center row of the array. The center element actually has a reflection coefficient greater than unity, which implies

that it absorbs power from some of the other elements. In other words, the left-hand dipoles in Fig. 4 radiate power, some of which is delivered to the right-hand array elements through the strongly-excited guided wave on the structure.For this particular scan angle, most of the elements are not matched, showing the scan blindness effect, yet a few near the array edges still have relatively low reflection coefficients. These results for the reflection coefficient show very good agreement with previously published results for this array [17, Fig. 4].

Table 1: Matrix setup (fill) and solve times for GIFFT and standard MoM for several structures.

	Fill Time [s]	Solve Time [s]	Number Iterations	Average % Error
Dipoles in Free Space	608.0	1591.2	309	---
GIFFT	4.2	232.0	263	0.20
GIFFT w/ preconditioner	4.2	7.2	7	0.19
Dipoles on Grounded Substrate	4698.6	4297.1	833	---
GIFFT	47.1	1132.7	911	0.15
GIFFT w/ preconditioner	47.6	23.2	17	0.15
Square Patches in Free Space	4391.8	53612.1	463	---
GIFFT	27.7	1100.5	340	0.96
GIFFT w/ preconditioner	27.0	32.0	9	0.97

B. Array of Patch Antennas Excited by Slots

The final case considered is an array of elements that are geometrically more complex, as shown in Fig.2, and the meshed patch, slot and microstrip are shown in Fig. 5. Two cases are considered: and array of 8×8 and a larger one of 25×25 element. The array elements are arranged on a rectangular lattice with periods $S_1 = S_2 = 30$ [mm]. The square conducting patches with dimensions $24.5\,[\text{mm}] \times 24.5\,[\text{mm}]$ are placed on a grounded dielectric substrate with $\varepsilon_r = 2.17$ and height =3 [mm]. The feeding slot has dimensions $10\,[\text{mm}] \times 1.5\,[\text{mm}]$ and is located 5.25 [mm] off the center of the patch. The microstrip under the ground plane has a width of 1.6 [mm], and a length of 17 [mm] that includes an open stub of length 10 [mm]. The microstrip substrate has $\varepsilon_r = 2.17$ and a thickness of 0.5 [mm]. The microstrip lines are excited by delta gap voltage generators and the operating frequency is 3.7 GHz. The design is not optimized to minimize the input impedance over a certain band, but is merely intended to illustrate the effectiveness of our new method. Each patch, slot and microstrip is meshed using quadrilaterals, creating 128 unknowns per array element as shown in Fig. 5. The GIFFT method used fourth-order interpolating polynomials in both planar directions.

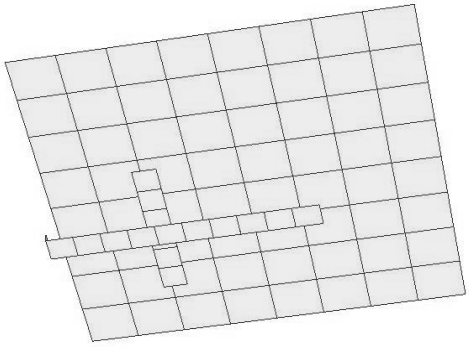

Fig. 5. Mesh of the square patch, slot and microstrip of one of the array elements. The ground plane surrounding the slot and the dielectric layers are not shown.

Table 1 shows the run times for the standard MoM and GIFFT solution of the array. It can be clearly seen that the GIFFT method offers a dramatic savings in both setup and solve times while maintaining a high level of accuracy. In this case the BiCGstab iterations are stopped when the algorithm's relative solution error falls below 0.5×10^{-4} to limit the overall simulation time. Also in this case it is seen that the use of the preconditioner dramatically reduces the number of BiCGstab iterations needed for a solution, further reducing solution time. For the larger 25x25elements array the iterations are stopped when the error falls below 10^{-2}.

As in the previous cases, the memory storage requirements are dramatically reduced by GIFFT. For example, for the $M = 625 = 25 \times 25$ square patch array, each element is discretized using N =128 basis functions (112 on the patch, 5 on the slot and 11 on the microstrip), requiring a storage of $N \times N$ =16384 complex numbers for *each* $\mathbf{p}, \mathbf{p}'$ block $\left[Z_{mn}^{\mathbf{pp}'} \right]$ of the impedance matrix. Instead, using GIFFT with a fourth-order interpolation scheme, requiring $r_1 \times r_2 = 5 \times 5 = 25$ sampling points per cell, only 16 distinct Green's function samples per cell are stored. For the layered medium considered here, this number must be multiplied by seven, the number of unique dyadic and scalar potential terms used in the mixed-potential formulation. The GIFFT storage advantage is further amplified by the fact that for $M = 625$ array elements in the square array, there are $M^2 = 390625$ matrix blocks in the complete matrix (which is why a Toeplitz fill was used instead), while there are only about $4M = 2500$ blocks of sampled Green's function points. For the 25×25 array, this means that the system matrix

for a standard MoM must contain about $117 \times 117 \times M^2 + 16 \times 16 \times M = 5.3 \times 10^2$ complex entries; this reduces to $117 \times 117 \times (2M - 1) + 16 \times 16 \times M = 17.1 \times 10^6$ when stored in the Toeplitz format. By contrast, there are only $7 \times 16 \times 4 \times M = 280 \times 10^3$ entries in the sampled Green's function array in addition to those relative to the self blocks and difference matrix (see (2)) that also grow as *M*.

Table 2: Matrix setup (fill) and solve times for GIFFT and standard MoM.

Array of patches with slots and microstrip lines (Fig.2)	Setup Time [s]	Solve Time [s]	Number Iterations	Average % Error
Array 8x8				
MoM w/ Toeplitz fill w/o precond.	1797	12551	2373	---
GIFFT w/o precond.	240	4627	2473	0.55
GIFFT w/ precond.	240	36	19	0.55
Array 25x25				
MoM w/ Toeplitz fill w/ precond.	≈ 9 hr	≈ 11 min per sing BiCGstab iteration	>100 program stopped before end	---
GIFFT w/ precond.	≈ 25 min	≈ 4 min (14s per iteration)	17	

VI. CONCLUSION

The GIFFT method for solving large array problems [1] is extended here to arbitrary arrays of printed elements in a layered material with the possible slot feeds. A block diagonal preconditioner has been tested and found to greatly improve the solution time by reducing the number of iterations required by the BiCGstab solver. The examples presented show the advantages of the method in reducing the memory requirements of the MoM matrix, as well as in reducing setup and solution times. A multiport analysis of such arrays can thus be performed in reasonable time even for large array structures. An extension of the GIFFT algorithm for arrays of cavity-backed patch antennas is currently under progress.

REFERENCES

[1] B. J. Fasenfest, F. Capolino, D. R. Wilton, D.R. Jackson, and N. Champagne, "A fast MoM solution for large arrays: Green's function interpolation with FFT," *IEEE Antennas and Wireless Propagation Letters,* Vol. 3, pp. 161-164, 2004.

[2] E. Bleszynski, M. Bleszynski, and T. Jaroszewicz, "AIM: Adaptive integral method for solving large scale electromagnetic scattering and radiation problems," *Radio Sci.*, Vol. 31, No. 5, pp. 1225-1251, 1996.

[3] S-Q Li, Y. Yu, C. H. Chan, K. F. Chan, and L. Tsang, "A sparse-matrix/canonical grid method for analyzing densely packed Interconnects," *IEEE Trans. Microwave Theory Tech.,* Vol. 49, No. 7, pp. 1221-1228, July 2001.

[4] L. Tsang; C. H. Chan, P. Kyung, and H. Sangani, "Monte-Carlo simulations of large-scale problems of random rough surface scattering and applications to grazing incidence with the BMIA/canonical grid method," *IEEE Trans. Antennas Propagat.,*, Vol. 43, No. 8, Aug. 1995.

[5] S. M. Seo, and J. F. Lee, "A fast IE-FFT algorithm for solving PEC scattering problems," *IEEE Trans. on Magnetics,* Vol. 41, No. 5, pp. 1476 – 1479, May 2005.

[6] A. Mori, F. De Vita, and A. Freni, "A modification of the canonical grid series expansion in order to increase the efficiency of the SMCG method," *IEEE Geoscience and Remote Sensing Letters,* Vol. 2, No. 1, pp. 87-89 Jan. 2005.

[7] R. Coifman, V. Rokhlin, and S. Wandzura, "The fast multipole method for the wave equation: A pedestrian prescription," *IEEE Antennas Propagat. Mag.*, Vol. 35, No. 3, pp. 7-12, June 1993.

[8] W. C. Chew, J.-M. Jin, C.-C. Lu, E. Michielssen, and J. M. Song, "Fast solution methods in electromagnetics," *IEEE Trans. Antennas Propagat.,* Vol. 45, No. 3, pp. 533 – 543, March 1997.

[9] J. Song, C.-C. Lu, and W. C. Chew, "Multilevel fast multipole algorithm for electromagnetic scattering by large complex objects", *IEEE Trans. Antennas Propagat.,* Vol. 45, No. 10, pp. 1488 – 1493, Oct. 1997.

[10] R. W. Kindt and J. L. Volakis, "Array decomposition-fast multipole method for finite array analysis," *Radio Sci.,* Vol. 39, RS2018, 2004.

[11] A. Neto, S. Maci, G. Vecchi, and M. Sabbadini, "Truncated Floquet wave diffraction method for the full wave analysis of large phased arrays. Part I and II," *IEEE Trans. Antennas Propagat.*, Vol. 48, No. 4, pp. 594-611, April 2000.

[12] O. A. Civi, P.H. Pathak, H-T. Chou, and P. Nepa, "A hybrid uniform geometrical theory of diffraction-moment method for efficient analysis of electromagnetic radiation/scattering from large finite planar arrays," *Radio Science*, Vol. 32, No. 2, pp. 607-620, March-April, 2000.

[13] F. Capolino, M. Albani, S. Maci, and L. B. Felsen, "Frequency-domain Green's function for a planar

periodic semi-infinite phased array. Part I and II," *IEEE Trans. Antennas and Prop.*, Vol. 48, No. 1, pp. 67 – 85, Jan. 2000.

[14] K. A. Michalski, and D. Zheng, "Electromagnetic scattering and radiation by surfaces of arbitrary shape in layered media. I. Theory," *IEEE Trans. Antennas Propagat.*, Vol. 38, No. 3, pp. 335-344, March 1990.

[16] S. M. Rao, D. R. Wilton, and A. W. Glisson, "Electromagnetic scattering by surfaces of arbitrary shape," *IEEE Transactions on Antennas and Propagation*, Vol. AP-30, No. 3, pp. 409-418, May 1982.

[17] W. A. Johnson, R. E. Jorgenson, L. K. Warne, J. D. Kotulski, J. B. Grant, R. M. Sharpe, N. J. Champagne, D. R. Wilton, and D.J. Jackson, "Our experiences with object-oriented design, FORTRAN 90, and massively parallel computations," *1998 Digest USNC/URSI National Radio Science Meeting*, p. 308, June 21-26, Atlanta, GA, 1998.

[18] D. M. Pozar, "Analysis of finite phased arrays of printed dipoles," *IEEE Trans. Antennas Propagat.*, Vol. 33, No. 10, pp. 1045-1053, Oct. 1985.

[19] D. M. Pozar, and D. H. Schaubert, "Analysis of an infinite array of rectangular microstrip patches with idealized probe feeds," *IEEE Trans. Antennas Propagat.*, Vol. 32, No. 10, pp. 1101-1107, Oct. 1984.

Bejamin. J. Fasenfest was born in Sacramento, CA, in 1980. He received the B.S. (summa cum laude) from the University of Houston in 2002, where an undergraduate research fellowship funded his research of dielectric resonator antennas. He was awarded a Tau Beta Pi fellowship, and continued on to a M.S. at the University of Houston in 2004, with a thesis on fast methods for large arrays. From 2004 to the present, he has worked at Lawrence Livermore National Laboratory, where his research interests include computational electromagnetics and electromagnetics modeling, from statics to terahertz.

Filippo Capolino was born in Florence, Italy, in 1967. He received the Laurea degree (cum laude) in electronic engineering and the Ph.D. degree, from the University of Florence, Italy, in 1993 and 1997, respectively. He has been a Research Associate until 2002 at the Dept. of Information Engineering, University of Siena, Italy, where he is presently an Assistant Professor. From 1997 to 1998, he was a Fulbright Research Visitor with the Dept. of Aerospace and Mech. Engineering, Boston University, MA, where he continued his research with a Grant from the Italian National Research Council (CNR), from 1998 to 1999. From 2000 to 2001 he was Research Assistant Visiting Professor with the Department of Electrical and Comp. Engineering, University of Houston, TX, where he is now an Adjunct Assistant Professor. In Nov.-Dec- 2003 he was an Invited Assistant Professor at the Institut Fresnel, France. His primary research interests include array antennas, periodic structures, numerical modeling, and metamaterials. He is the coordinator of the Siena Unit for the Network of Excellence "Metamorphose" on Metamaterials of the EU sixth framework program.

Dr. Capolino was awarded with a MMET'94 Student Paper Competition Award in 1994, the Raj Mittra Travel Grant for Young and Senior Scientists in 1996, and 2006, respectively, the "Barzilai" prize for the best paper at the National Italian Congress of Electromagnetism (XI RiNEm) in 1996, and a Young Scientist Award for participating at the URSI Int. Symp. Electromagn. Theory in 1998. He received the R.W. P. King Prize Paper Award from the IEEE Antennas and Propagation Society for the Best Paper of the Year 2000, by an author under 36. He is an Associate Editor for the IEEE Transactions on Antennas and Propagation.

Donald R. Wilton was born in Lawton, OK, October 25, 1942. He received the B.S., M.S., and Ph.D. degrees from the University of Illinois, Urbana-Champaign, in 1964, 1966, and 1970, respectively.

From 1965 to 1968 he was with Hughes Aircraft Co., Fullerton, CA, engaged in the analysis and design of phased array antennas. From 1970–1983 he was with the Department of Electrical Engineering, University of Mississippi, and since 1983 he has been Professor of Electrical Engineering at the University of Houston. From 1978–1979 he was a Visiting Professor at Syracuse University. During 2004-2005 he was a visiting professor at the Polytechnic of Turin, Italy, the Sandia National Laboratories, and the University of Washington. His primary research interest is in computational electromagnetics, and he has published, lectured, and consulted extensively in this area.

Dr. Wilton is a Fellow of the IEEE and received the IEEE Third Millenium Medal. He has served the IEEE Antennas and Propagation Society as an Associate Editor of the Transactions on Antennas and Propagation, as a Distinguished National Lecturer, and as a member of AdCom. Dr. Wilton is also a member of Commission B of URSI, in which he has held various offices including Chair of U. S. Commission B.